

Chemical abundance analysis of red giant branch stars in the globular cluster E3[★]

L. Monaco¹, S. Villanova², G. Carraro³, A. Mucciarelli^{4,5} and C. Moni Bidin⁶

¹ Departamento de Ciencias Físicas, Universidad Andres Bello, Fernandez Concha 700, Las Condes, Santiago, Chile; e-mail: lorenzo.monaco@unab.cl

² Universidad de Concepción, Casilla 160-C, Concepción, Chile

³ Dipartimento di Fisica e Astronomia Galileo Galilei, Vicolo Osservatorio 3, I-35122, Padova, Italy

⁴ Dipartimento di Fisica e Astronomia, Università degli Studi di Bologna, via Gobetti 93/2, I-40129 Bologna, Italy

⁵ INAF - Osservatorio di astrofisica e scienza dello spazio di Bologna, Via Gobetti 93/3, I-40129, Bologna, Italy

⁶ Instituto de Astronomía, Universidad Católica del Norte, Av. Angamos 0610 Antofagasta, Chile

Received ...; Accepted...

ABSTRACT

Context. Globular clusters are known to host multiple stellar populations, which are a signature of their formation process. The globular cluster E3 is one of the few low-mass globulars that is thought not to host multiple populations.

Aims. We investigate red giant branch stars in E3 with the aim of providing a first detailed chemical inventory for this cluster, we determine its radial velocity, and we provide additional insights into the possible presence of multiple populations in this cluster.

Methods. We obtained high-resolution FLAMES-UVES/VLT spectra of four red giant branch stars likely members of E3. We performed a local thermodynamic equilibrium abundance analysis based on one-dimensional plane parallel ATLAS9 model atmospheres. Abundances were derived from line equivalent widths or spectrum synthesis.

Results. We measured abundances of Na and of iron peak (Fe, V, Cr, Ni, Mn), α (Mg, Si, Ca, Ti), and neutron capture elements (Y, Ba, Eu). The mean cluster heliocentric radial velocity, metallicity, and sodium abundance ratio are $v_{helio}=12.6\pm 0.4\text{ km s}^{-1}$ ($\sigma=0.6\pm 0.2\text{ km s}^{-1}$), $[\text{Fe}/\text{H}]=-0.89\pm 0.08\text{ dex}$, and $[\text{Na}/\text{Fe}]=0.18\pm 0.07\text{ dex}$, respectively. The low Na abundance with no appreciable spread is suggestive of a cluster dominated by first-generation stars in agreement with results based on lower resolution spectroscopy. The low number of stars observed does not allow us to rule out a minor population of second-generation stars. The observed chemical abundances are compatible with the trends observed in Milky Way stars.

Key words. Stars: abundances – Stars: atmospheres – (Galaxy:) globular clusters: individual: E3

1. Introduction

Once considered a prototype of simple stellar populations (Renzini & Fusi Pecci 1988), globular clusters (GCs) are now known to host multiple stellar populations (MPs). First discovered in red giant branch (RGB, e.g., Cohen 1978) stars, chemical inhomogeneities in light elements persist down to the cluster main sequence (MS, Gratton et al. 2001) stars. The low central temperatures and thin convective envelopes of these low-mass stars make them unable to be the source of the observed abundance variations, which were then recognized as signatures of the GCs formation process.

Globular clusters usually host at least two stellar populations, one with a composition compatible with halo field stars (first generation, FG) and the other with an enriched or polluted composition (second generation, SG). The observed abundance spread, most notably the Na-O (Carretta et al. 2009a,b) and C-N (Pancino et al. 2010) anti-correlations, accompanied sometimes by Mg-Al anti-correlations (Pancino et al. 2017) and He abundance variations (Pasquini et al. 2011), are suggestive of hot hydrogen burning. One of the main questions yet to be answered is the nature of the polluters which gave rise to enriched stars. Several models have been proposed including pollution from

massive asymptotic giant branch stars (D’Ercole et al. 2016) and fast rotating massive stars (Decressin et al. 2007), among others (Bastian & Lardo 2017). However, none of the models is fully satisfactory (Renzini et al. 2015) and in some cases, different polluters may also be required (Carretta et al. 2018).

Most GCs present a Na-O anti-correlation and are dominated by SG stars. The fraction of stars belonging to the FG increases, however, with decreasing cluster mass (Milone et al. 2017). The most massive open clusters and the least massive globular clusters were both investigated in order to find empirical evidence about the mass limit for the formation of multiple populations (Bragaglia et al. 2012). A few low-mass GCs do not present evidence of multiple populations (Cohen 2004; Sbordone et al. 2007), the most massive being Rup 106 (Villanova et al. 2013). Nonetheless, MPs are detected in the less massive GCs NGC 6362, NGC 6535, and ESO452-SC11 (Dalessandro et al. 2014; Mucciarelli et al. 2016; Bragaglia et al. 2017; Simpson et al. 2017). In addition to mass, the age and metallicity may be two additional relevant parameters (Carretta et al. 2010). In particular, massive clusters older than $\sim 2\text{ Gyr}$ are observed to host MPs, while younger ones are not (see Martocchia et al. 2017, 2018; Bastian & Lardo 2017, and references therein).

With an absolute total magnitude of $M_V=-4.12$, E3 (α , $\delta = 09:20:57.07$, $-77:16:54.8$; Harris 1996, 2010 edition) is one of

[★] Based on observations made with ESO Telescopes at the La Silla Paranal Observatory under programme ID 097.D-0056(A).

the faintest globular clusters in the Galaxy and likely one of the least massive ($1.4 \times 10^4 M_{\odot}$; Salinas & Strader 2015). Its color magnitude diagram, with all the evolutionary phases beyond the MS severely contaminated by field stars, as expected from its location ($l = 292^{\circ}.270$, $b = -19^{\circ}.020$), made this cluster a particularly difficult one to be studied.

Recently, two low-resolution spectroscopy studies on E3 have been published: Salinas & Strader (2015, hereafter SS15) and de la Fuente Marcos et al. (2015, hereafter FM15). SS15 found no evidence for multiple stellar populations in this cluster from the study of the strengths of the CH-CN bands of low-resolution spectra of 23 red giant branch stars. FM15 have analyzed low-resolution, medium signal-to-noise ratio (S/N) spectra of nine stars, finding two probable members and have derived tentative radial velocity (RV) and metallicity estimates of $45 \pm 5 \text{ km s}^{-1}$ and $[\text{Fe}/\text{H}] = -0.7$ dex. SS15, instead, have derived a RV of $8.9 \pm 2.8 \text{ km s}^{-1}$. Both of these RV determinations are based on just two stars and are obviously in conflict with each other. Robust determinations of its metallicity, RV, and tangential velocity are essential to derive the cluster actual location and motion and possibly associate E3 with other clusters (FM15).

We present here the first chemical abundance analysis of a sample of RGB stars belonging to E3 based on high-resolution spectroscopy. In section §2 we present the observations and data reduction. Sections §3 and §4 present the performed abundance analysis and the obtained results. Finally, in §5 we present our conclusions.

2. Observations and data reduction

Observations were conducted using the multi-object, fiber fed FLAMES facility (Pasquini et al. 2002) mounted at the unit two telescope (UT2, “Kueyen”) of the European Southern Observatory (ESO) Very Large Telescope (VLT) located in the Chilean Andes. FLAMES allows the simultaneous observation of up to seven or eight objects (depending on the plate used for the observations) using the red arm of the high-resolution UV-Visual Echelle Spectrograph (UVES, Dekker et al. 2000). FLAMES-UVES observations deliver spectra with a resolution of $R \approx 47,000$.

We observed seven stars using FLAMES-UVES, set at central wavelength 580 nm, which covers the spectral range 476–684 nm, with a 5 nm gap around the central wavelength. One fiber was placed on an empty field for the purpose of sky subtraction. Three 3000 s exposures were taken in service mode on the nights of April 25, May 19, and May 21, 2016.

Table 1 lists the target stars identification numbers, coordinates, and V- and I-band photometry. Only two 3000 s observations were obtained for object #132. The seven stars observed are plotted as filled symbols in the V versus V-I E3 color magnitude diagram (CMD) in Figure 1 (upper left panel). We adopt here the photometry described in FM15. Star #100 excluded, our targets are all present in the Veronesi et al. (1996, hereafter V96) photometry. For comparison, the color difference between the V96 V-I and ours are below 0.01 mag for all stars but #1. In this case the V96 V-I color is 0.028 mag smaller than ours. This difference corresponds to a temperature about 50 K hotter when using the color to get the stellar effective temperature, well below the typical temperature errors assumed in chemical abundance analysis. A 13 Gyr isochrone of metallicity $Z=0.003$ from the PARSEC collection¹ (Bressan et al. 2012) was superposed to the cluster CMD, adopting $E(V-I)=0.47$ and $(m-M)_V=15.07$

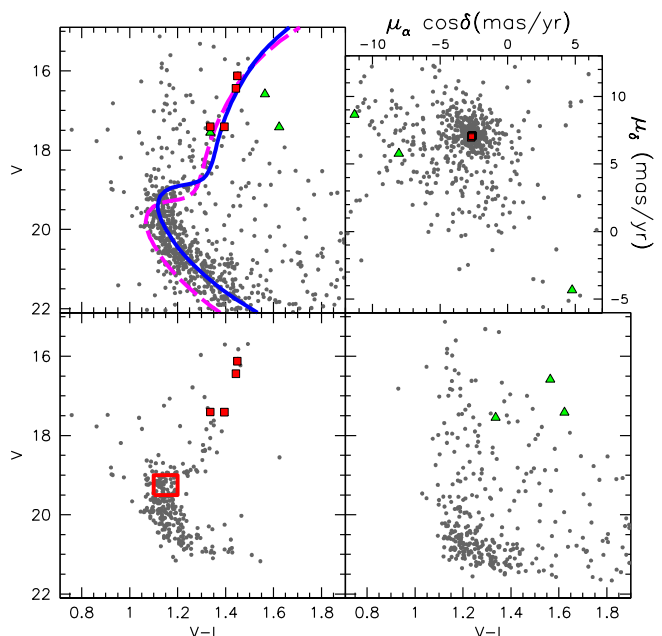


Fig. 1. Upper left panel: E3 V vs V-I color magnitude diagram. Target stars are marked by large filled symbols. Filled red squares are E3 radial velocity members. The continuous and dashed lines are $Z=0.003$, 13 Gyr isochrones from the PARSEC collection (Bressan et al. 2012) where the visual distance modulus and reddening are the values we adopt here from FM15 (continuous blue line) or from Harris (1996, 2010 revision, dashed magenta line). Upper right panel: Gaia DR2 proper motions of stars cross-identified from the photometry in the upper left panel. RV members (red filled squares) have very similar PMs, and thus are almost superposed on each other in the figure. Lower left panel: CMD of stars having PMs within three times the errors from the mean E3 PM. Stars in the cross-identified catalog and having $19.0 < V < 19.5$; $1.1 < V-I < 1.2$ (red box) were used to select the MS stars that were used to define the cluster mean PM. Lower right panel: CMD of stars having PMs exceeding three times the errors from the mean E3 proper motion.

from FM15 (our favored values, continuous blue line) and $E(V-I)=0.42$ and $(m-M)_V=15.47$ from Harris (1996, 2010 edition, dashed magenta line). The Schlegel et al. (1998) reddening maps suggest that E3 is not significantly affected by differential reddening. The mean reddening at the positions of the seven stars we observed is $E(B-V)=0.340 \pm 0.005$ or $E(B-V)=0.293 \pm 0.004$, according to Schlafly & Finkbeiner (2011) with the maximum variation among the positions on the order of 0.01 mag. We note that Sarajedini et al. (2007) suggest for E3 an age that is ~ 2 Gyr younger than 47 Tuc. As can be seen from Fig. 3 of de la Fuente Marcos et al. (2015), at these old ages, differences of a few Gyr are fully compatible with our photometry. On the other hand, Marín-Franch et al. (2009) classify E3 among the group of “old” globular clusters (12.8 ± 1.4 Gyr in their D07 scale) and did not find a significantly younger age with respect to 47 Tuc (13.1 ± 0.9 Gyr in the same scale).

Raw science data were retrieved through the ESO data archive² together with the associated master calibrations as delivered by the system. Raw data were then reduced using those calibrations and the FLAMES-UVES CLP based pipeline version 5.5.5³. The “flames_obs_scired” recipe alone was applied.

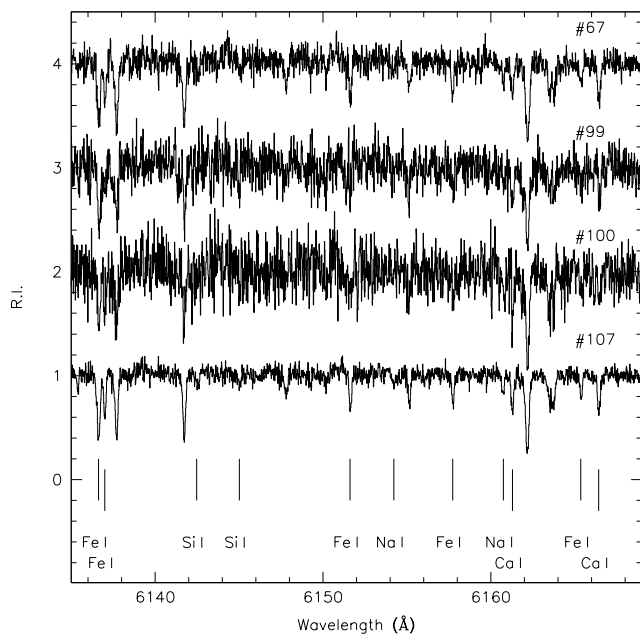
² <http://archive.eso.org/>

³ <http://www.eso.org/sci/software/pipelines/>

¹ http://stev.oapd.inaf.it/cgi-bin/cmd_2.8

Table 1. Target IDs, coordinates, photometry, atmospheric parameters, measured metallicities, spectral S/N, radial velocities and Gaia DR2 proper motions.

ID	α (J2000)	δ (J2000)	V	V-I	T_{eff} K	$\log g$	ξ km s ⁻¹	[Fe/H]	S/N @600nm	V_{helio} km s ⁻¹	$\mu_{\alpha} \cos \delta$ mas/yr	μ_{δ} mas/yr
1	09:20:50.59	-77:19:55.7	17.55	1.34					8	-0.2±0.6	-11.32±0.11	8.66±0.12
67	09:21:15.65	-77:18:04.0	16.44	1.44	4807	2.53	1.29	-0.89	14	11.8±1.0	-2.69±0.06	6.95±0.06
99	09:21:01.01	-77:16:34.3	17.41	1.34	5047	3.04	1.16	-0.82	10	13.3±0.1	-2.62±0.11	7.09±0.12
100	09:21:50.61	-77:16:34.1	17.41	1.39	4923	2.98	1.17	-0.84	8	12.8±1.2	-2.62±0.11	7.08±0.11
107	09:20:16.73	-77:15:56.9	16.12	1.45	4785	2.39	1.32	-1.01	24	12.3±0.8	-2.67±0.06	7.07±0.05
121	09:20:21.89	-77:18:47.8	16.58	1.56					11	39.1±3.9	4.78±0.07	-4.34±0.07
132	09:20:45.94	-77:15:12.8	17.42	1.62					8	29.0±0.7	-8.05±0.12	5.77±0.13

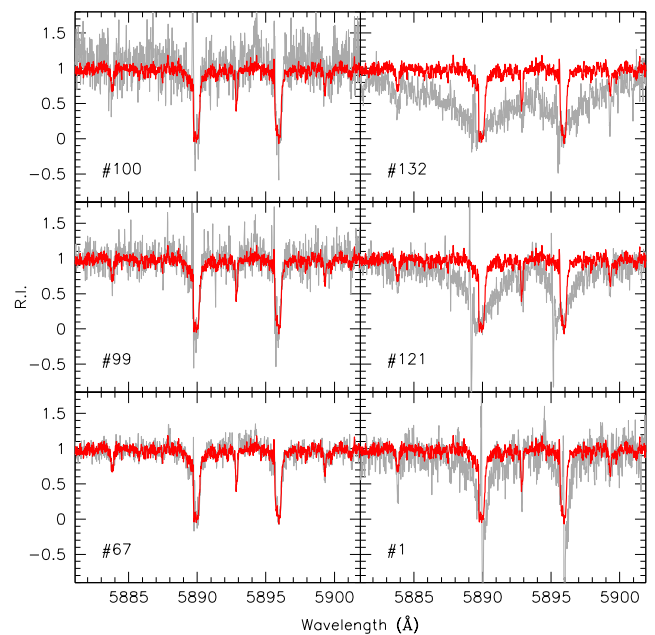

Fig. 2. Sample of the spectra of the observed stars. A few absorption lines of different elements are indicated.

For each exposure, the spectrum corresponding to the sky position was subtracted from the individual stellar spectra.

For each star and epoch, the RV was measured using the `fxcor` task within IRAF⁴ to cross-correlate the observed spectra with a template synthetic spectrum selected from the Coelho et al. (2005) collection. Heliocentric corrections were calculated using the `rvcorrect` task in IRAF. Finally, individual stellar spectra were corrected to rest frame and median combined. The signal-to-noise ratios measured on the combined spectra at about 600nm are also given in Table 1 together with the mean heliocentric radial velocity. The errors reported on the RVs are the standard deviation of the available measurements. Figure 2 presents a sample of the obtained spectra, with a few absorption lines marked for reference.

Stars #67, #99, #100, and #107 have very similar RVs, significantly different from the remaining three stars. The locations of these four stars in the CMD in Figure 1 (upper left panel, red

⁴ IRAF is distributed by the National Optical Astronomy Observatory, which is operated by the Association of Universities for Research in Astronomy (AURA) under a cooperative agreement with the National Science Foundation.


Fig. 3. Sample of the spectra of the observed stars in the region of the NaD doublet. The spectrum of star #107 is marked in red and superposed on the spectra of the other stars (gray). The spectra of stars #1, #121, and #132 present significantly broader NaD lines than stars #67, #99, #100, and #107.

filled squares) are compatible with the expected location of the cluster RGB (continuous blue line). The position of star #1 is also compatible with the cluster RGB. Its RV is, however, significantly different from that of the other four stars. We show in Figure 3, a portion of the stellar spectra, centered around the sodium D doublet (NaD). The spectrum of star #107 (thick continuous red line) is superposed on the spectra of the stars indicated in each subpanel (continuous gray lines). The shape of the NaD lines is very similar for stars #67, #99, #100, and #107 (left panels). On the other hand, the spectrum of star #1 has significantly broader NaD lines (bottom right panel) even though it has the same color as star #99. This suggests that the observed line broadening is a pressure effect, and that star #1 is a dwarf star rather than a giant. The spectra of stars #121 and #132 present very broad NaD lines (top and middle right panels). This is expected, however, given their redder color and cooler temperatures with respect to the remaining stars. Pressure effects are therefore not easily disentangled.

We cross-identified stars in our reference photometry with the Gaia DR2 catalog (Gaia Collaboration et al. 2016, 2018) using the TOPCAT code (Taylor 2005). The upper right panel of Fig. 1 shows the proper motions (PM) measured by the Gaia mission; our target stars are identified with the same symbols as in upper left panel. Stars #67, #99, #100, and #107 (RV members, red filled squares) also present very similar PMs, while stars #1, #121, and #132 have significantly scattered values. Using our photometry, we selected E3 main sequence stars using the box shown for reference in the lower left panel ($19.0 < V < 19.5$; $1.1 < V-I < 1.2$). We also required errors in PM lower than 0.5 mas/yr and differences between the V and g magnitudes in the range from -0.35 to -0.10, according to the corresponding distributions. We further excluded one outlier from the resulting PM distributions. This way, we selected 44 likely cluster member MS stars, from which we obtain a mean E3 PM of $(\mu_\alpha \cos \delta; \mu_\delta) = (-2.71 \pm 0.40; 7.20 \pm 0.46)$ mas/yr. The lower panels of Fig. 1 present the CMDs of stars having PMs within (left) or exceeding (right) three times the quoted errors from the mean cluster PM. The Gaia PMs allow us to nicely distinguish the E3 cluster population, clearly visible in the lower left panel, from the contaminating field stars (lower right panel). We note that the four RV members have PMs fully compatible with the cluster PM derived from MS stars (lower left and upper right panels, see also Table 1). We therefore consider that stars #1, #121, and #132 are not cluster members.

Considering only stars #67, #99, #100, and #107 as members, we obtain a mean cluster radial velocity and dispersion of $v_{helio} = 12.6 \pm 0.4 \text{ km s}^{-1}$ and $\sigma = 0.6 \pm 0.2 \text{ km s}^{-1}$, where the errors were in both cases evaluated through a jackknife re-sampling technique (Lupton 1993). The cluster mean RV we obtained is in reasonable agreement with SS15, who measured $8.9 \pm 2.8 \text{ km s}^{-1}$ from intermediate-resolution (0.75 \AA) optical spectroscopy ($\sim 5100\text{--}5600 \text{ \AA}$) of two stars. On the other hand, FM15 measured $45 \pm 5 \text{ km s}^{-1}$, which suggests the two stars they measured to be likely non-cluster members. Even though it is among the clusters with the largest binary fraction (Veronesi et al. 1996; Milone et al. 2012) and within the limitation of our reduced statistic, the E3 velocity dispersion is the smallest found in a globular cluster, after Pal 14 ($0.4 \pm 0.1 \text{ km s}^{-1}$), according to the Harris (1996, 2010 edition) catalog. This low σ supports a very low present day mass for E3, in agreement with the suggestion of SS15, who estimates a cluster mass of $1.4 \times 10^4 M_\odot$.

3. Abundance analysis

Chemical abundance analysis was performed on the spectra of stars #67, #99 #100, and #107 using the local thermodynamic equilibrium code MOOG⁵ (Snedden 1973). Appropriate one-dimensional ATLAS9 model atmospheres were calculated (Kurucz 1993a; Sbordone, Bonifacio, Castelli, & Kurucz 2004) for the analysis.

Stellar effective temperatures were derived from the V-I colors, using the Alonso et al. (1999) calibrations ($\sigma(T_{\text{eff}}) = 125 \text{ K}$). The V-I colors were converted to the Johnson system using the relation provided by Bessell (1983). We adopted $E(V-I) = 0.47$ from FM15. Had we used a reddening of $E(B-V) = 0.30 \text{ mag}$ or $E(V-I) = 0.42$ from Schlafly & Finkbeiner (2011), our temperatures would have resulted between 108–124 K colder (average 114 K). A reddening of $E(B-V) = 0.25 \text{ mag}$ or $E(V-I) = 0.35$ from the Schlegel et al. (1998) reddening maps corrected according

to Bonifacio et al. (2000) would correspond instead to $\sim 260 \text{ K}$ colder temperatures ($\Delta T_{\text{eff}} = 262 \pm 18 \text{ K}$). Surface gravities were obtained from the standard relation

$$\log g = \log \frac{M}{M_\odot} + 4 \log \frac{T_{\text{eff}}}{5777} + 0.4(M_{\text{bol}} - 4.76) + 4.44,$$

where we made use of the solar effective temperature, surface gravity, and bolometric absolute magnitudes of 5777 K, 4.44 dex, and 4.76 mag, respectively. The bolometric magnitudes were calculated from the visual values using again the apparent visual distance modulus from FM15, i.e., $(m-M)_V = 15.07$. The bolometric correction was obtained from the Alonso et al. (1999) calibration for the appropriate T_{eff} and metallicity, along with a stellar mass of $0.8 M_\odot$. A variation of 150 K in T_{eff} results in a change of about 0.07 dex in $\log g$.

The distance modulus we employed is 0.4 mag smaller than the value reported by Harris (1996), namely $(m-M)_V = 15.47$. A $Z = 0.003$, 13 Gyr old isochrone would not be a reasonable match to the cluster main sequence, if we used $(m-M)_V = 15.47$ and $E(V-I) = 0.42$ (dashed magenta line in Fig. 1, upper left panel) or $E(V-I) = 0.35$. We note that Sarajedini et al. (2007) obtained, from the analysis of their HST CMD, the same reddening value we adopt here. If we adopted this latter distance modulus, we would obtain surface gravities 0.16 dex lower. Finally, microturbulent velocities were obtained from the Marino et al. (2008) calibration: $\xi = -0.254 \log g + 1.930$. A variation of 0.2 dex in $\log g$ would cause a change of 0.05 km s^{-1} in ξ .

In the analysis, we employed the same line list we used in other publications of our group (see, e.g., Villanova et al. 2016) and we refer the reader to Villanova & Geisler (2011) for details. Abundances were derived from line equivalent widths (EWs) for Fe, Na, Si, Ca, Ti, Cr, and Ni and through spectroscopy for Mg, V, Mn, Y, Ba, and Eu.

The measured iron abundances are listed in Tables 1 and 2. Table 2 also gives the species over iron abundance ratios, the adopted solar abundances, and the mean species abundance and Gaussian dispersion for the sample when the abundance was measured for more than one star. For each star and species we give the error of the mean (when more than one line was used) and the number of lines used. An “s” indicates whether the line was measured via spectroscopy.

Following Cayrel (1988), given the resolution and sampling of our spectra, we expect errors on the measured EWs to be on the order of $\sim 4\text{--}11 \text{ m\AA}$, depending on the spectral S/N. We considered a line as detected if its EW exceeds the corresponding uncertainty by at least three times. Program stars have similar atmospheric parameters (see Table 1). Table 3 presents the abundance changes resulting for variations in the atmospheric parameters of $\Delta T_{\text{eff}} = \pm 150 \text{ K}$, $\Delta \log g = 0.2 \text{ dex}$, and $\Delta \xi = \pm 0.05 \text{ km s}^{-1}$, taken as representative of the internal uncertainties. We note, however, that temperatures 260 K colder than those we adopted would correspond to about 0.28 dex lower metallicities. We also allow for an uncertainty in the measured iron abundance of $\pm 0.15 \text{ dex}$. When the abundance was derived from at least three lines, we consider the error of the mean listed in Table 2 as representative of the error induced by the spectral S/N. For elements derived from one or two lines only, this uncertainty is set to the error returned by the fitting procedure when the abundance was obtained through spectroscopy, or to the abundance uncertainty induced by a variation in EW equal to the values mentioned above, following Cayrel (1988). We list under column $\epsilon(S/N)$ the minimum and maximum observed values. Given the limited and different quality of the stellar spectra under analysis,

⁵ <http://www.as.utexas.edu/~chris/moog.html>

Table 2. Target stars chemical abundances. The penultimate column lists average abundances and Gaussian dispersions. The adopted solar abundances are given in the last column. Numbers in parentheses indicate the error of the mean and the number of lines used. An “s” character after the second number in parentheses is used to indicate a measure performed through spectroscopy. Star #100 was excluded from the computation of the mean iron abundance and dispersion from Fe II lines.

Element	#67	#99	#100	#107	<[X/Y]> ±σ	A(X) _⊙
[FeI/H]	-0.89 (0.01/56)	-0.82 (0.03/42)	-0.84 (0.03/51)	-1.01 (0.01/63)	-0.89±0.08	7.50
[FeII/H]	-0.85 (0.05/5)	-0.74 (0.05/4)	-0.43 (0.08/5)	-1.04 (0.03/5)	-0.88±0.15	7.50
[Na/Fe]	0.12 (-/1)	0.17 (0.01/2)	0.29 (-/1)	0.16 (0.02/2)	0.18±0.07	6.37
[Mg/Fe]	0.13 (-/1s)	—	—	0.43 (-/1s)	0.28±0.21	7.54
[Si/Fe]	0.38 (0.06/2)	0.47 (0.07/2)	0.42 (0.01/2)	0.38 (0.05/4)	0.41±0.04	7.61
[Ca/Fe]	0.37 (0.03/4)	0.36 (0.08/4)	0.27 (0.11/4)	0.36 (0.02/5)	0.34±0.05	6.39
[Ti/Fe]	0.32 (0.02/5)	0.29 (0.05/3)	0.21 (-/1)	0.38 (0.03/8)	0.30±0.07	4.94
[V/Fe]	0.07 (-/1s)	—	—	0.22 (-/1s)	0.14±0.11	4.00
[Cr/Fe]	0.20 (-/1)	—	0.02 (-/1)	0.10 (-/1)	0.11±0.09	5.63
[Ni/Fe]	0.05 (0.02/10)	0.03 (0.08/5)	-0.04 (0.09/6)	0.02 (0.02/8)	0.01±0.04	6.26
[Mn/Fe]	—	—	—	-0.22 (-/1s)	—	5.37
[Y/Fe] _{509nm}	—	—	—	-0.08 (-/1s)	—	2.25
[Y/Fe] _{540nm}	—	—	—	0.19 (-/1s)	—	2.25
[Ba/Fe]	0.01 (-/1s)	-0.06 (-/1s)	0.11 (-/1s)	0.07 (-/1s)	0.03±0.07	2.34
[Eu/Fe]	—	—	—	0.49 (-/1s)	—	0.52

in order to perform an analysis that is as homogeneous as possible for the sample stars, we decided to keep the T_{eff} , $\log g$, and ξ fixed at their initial values.

For the calculation of the abundance variations in Table 3, we adopted the atmospheric parameters and abundances of star #107. Uncertainties in the T_{eff} , $\log g$, and ξ are correlated and are summed directly. This is then summed in quadrature to the uncertainties in $A(\text{Fe})$ and from the spectral S/N. The penultimate column lists the overall abundance uncertainty for each species. Two values are provided corresponding to the minimum and maximum S/N error given in the previous column, when applicable. Finally, in the last column we list the observed Gaussian dispersion in the measured abundances when measures were performed for more than one star.

The iron abundances obtained from the Fe I and Fe II lines are in good agreement (differences lower than 0.1 dex) for stars #67, #100, and #107, lending support to the adopted gravities. For star #100, on the other hand, we find a 0.4 dex abundance difference. The higher iron abundance derived from Fe II lines may originate from an incorrect placement of the continuum in the low S/N (the lowest in the sample) spectrum of star #100 which might have lead to overestimate the EWs of the weak Fe II lines. Differences between the iron abundance derived from Fe I and Fe II lines have been reported for a few clusters that are thought to present an iron spread (see Mucciarelli et al. 2018, and references therein). In those cases, however, the differences were smaller and iron abundances based on Fe II lines are considered to be more reliable. In the case of star #100, this seems unlikely, and the iron content derived from Fe I lines should be considered more robust, due to the larger number of measured lines and the agreement with the iron abundance derived for the other stars in the sample from both Fe I and Fe II lines. A $\log g$ 0.4 dex lower for this star would decrease the $A(\text{FeII})$ and the $A(\text{Ba})$ abundances by about 0.18 and 0.12 dex, respectively, bringing in better agreement the iron abundances derived from Fe I and Fe II lines and the Ba abundance of this star with the values derived for the other stars. The mean iron abundance and dispersion from Fe II lines given in Tables 2 and 3 were computed excluding star #100. With the inclusion of this star we would obtain instead $[\text{Fe II}/\text{H}]=-0.76\pm 0.26$ dex.

4. Results

The observed species abundance spreads (last column in Table 3) are typically on the same order of or smaller than the expected uncertainties (penultimate column), due to the uncertainties in the atmospheric parameters and the spectral S/N.

We measured Na abundances between 0.12 and 0.29 dex, i.e., a 0.17 dex variation and a Gaussian dispersion of 0.07 dex, which is compatible with the expected measurement uncertainties. The studied cluster stars thus have homogeneous Na abundances within the allowed errors. Sodium abundances were corrected for departures from local thermodynamic equilibrium following Gratton et al. (1999). Unfortunately, in our spectra the 6300.3Å oxygen line is severely contaminated by a close, strong emission sky line. As a consequence, we were not able to measure or put an upper limit to the O abundance of the target stars.

In the left panel of Fig. 4 we present the Na-O anticorrelation for the collection of GCs studied by Carretta et al. (2009a,b, gray filled circles, upper limits excluded). Data for the GCs M4 and 47 Tuc having metallicities close to E3 are also marked as open red squares and magenta crosses, respectively. The short- and long-dashed horizontal lines indicate the separation between the first and second stellar generation in these clusters, as defined by Carretta et al. (2010). These limits are set 0.3 dex above the observed minimum Na abundance (or $[\text{Na}/\text{Fe}]_{\text{min}}+4\sigma$), excluding obvious outliers. In the right panel we present the corresponding data for the intermediate- and low-mass globular clusters NGC 288 ($M_V=-6.75$, Harris 1996), Ter 8 ($M_V=-5.07$ Carretta et al. 2014, stars with both O and Na measures only) and NGC 6535 ($M_V=-4.75$ Bragaglia et al. 2017, upper limits excluded). Finally, in the middle panel we show the Na abundances of E3 stars and the Ter 8 stars from Carretta et al. (2014) for which no O abundance was measured. E3 stars are placed in the lower portion of the diagram, which is populated by stars less enriched in Na. All of our E3 stars are close to or below the line separating FG and SG stars in M4 and 47 Tuc. Three out of four E3 stars are also very close to the line dividing FG and SG stars in the low- and intermediate-mass clusters NGC 288 and NGC 6535. In the case of Ter 8, Carretta et al. (2014) tentatively identified as belonging to the SG only the star

Table 3. Sensitivities of the derived abundances to the indicated variation of the atmospheric parameters. The last two columns indicate the combined total expected uncertainty and the observed dispersion from Table 2, respectively. Column $\epsilon(S/N)$ indicates the minimum and maximum abundance variation observed from Table 2 (error of the mean) or, when only one or two lines were measured, expected according to the EW error induced from the spectral S/N or as returned from the fitting procedure in the case of spectrum synthesis.

	ΔT_{eff} ± 150 K	$\Delta \log g$ ± 0.2 dex	$\Delta \xi$ $\pm 0.05 \text{ km s}^{-1}$	$\Delta A(\text{Fe})$ ± 0.15	$\epsilon(S/N)$	Total	Observed
[Fe I/H]	0.16	0.00	0.02	0.00	0.01 / 0.03	0.18	0.08
[Fe II/H]	0.06	0.09	0.01	0.00	0.03 / 0.08	0.16 / 0.18	0.15
[Na I/Fe]	0.05	0.00	0.02	0.01	0.07 / 0.18	0.10 / 0.19	0.07
[Mg I/Fe]	0.03	0.03	0.01	0.00	0.08 / 0.12	0.11 / 0.14	0.21
[Si I/Fe]	0.14	0.03	0.01	0.02	0.05 / 0.21	0.19 / 0.28	0.04
[Ca I/Fe]	0.00	0.01	0.01	0.01	0.02 / 0.11	0.03 / 0.11	0.05
[Ti I/Fe]	0.05	0.00	0.01	0.01	0.02 / 0.20	0.06 / 0.21	0.07
[V I/Fe]	0.06	0.00	0.02	0.02	0.13	0.15	0.11
[Cr I/Fe]	0.07	0.00	0.01	0.01	0.07 / 0.20	0.11 / 0.22	0.09
[Ni I/Fe]	0.02	0.02	0.01	0.01	0.02 / 0.09	0.05 / 0.10	0.04
[Mn I/Fe]	0.03	0.00	0.02	0.01	0.04	0.06	
[Y II/Fe] _{509nm}	0.11	0.06	0.00	0.04	0.12	0.21	
[Y II/Fe] _{540nm}	0.16	0.08	0.01	0.05	0.11	0.28	
[Ba II/Fe]	0.10	0.06	0.03	0.04	0.05 / 0.10	0.20 / 0.22	0.07
[Eu II/Fe]	0.16	0.08	0.01	0.05	0.11	0.28	

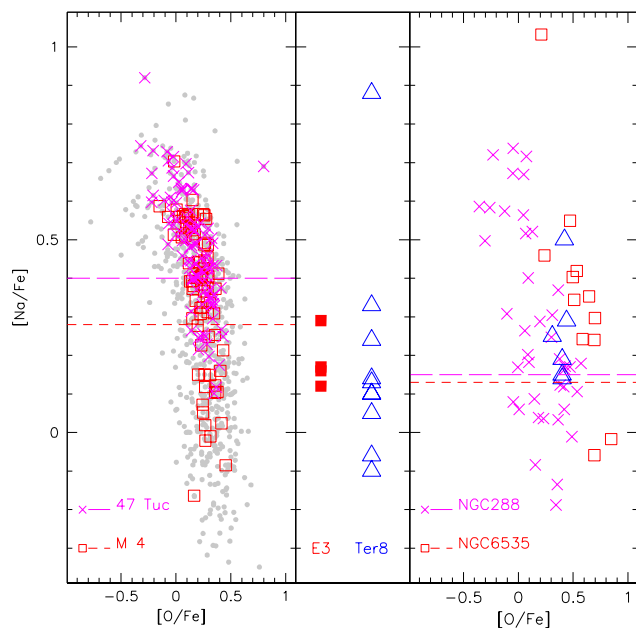


Fig. 4. Left panel: Na-O anti-correlation ($[\text{Na}/\text{Fe}]$ vs $[\text{O}/\text{Fe}]$) for the sample of GCs studied by Carretta et al. (2009a,b). M4 and 47 Tuc stars are marked as red open squared and magenta crosses, respectively. The short- long-dashed red and magenta lines indicate the separation between FG and SG stars in the two clusters, according to Carretta et al. (2010). Right panel: Same as left panel, but for NGC 288 (magenta crosses), Ter 8 (Carretta et al. 2014, open blue triangles for stars with both O and Na measures), and NGC 6535 (Bragaglia et al. 2017, upper limits excluded). Middle panel: E3 (filled red squares) and Ter 8 (Carretta et al. 2014, stars with Na measures only) Na abundances.

having the highest Na abundance ratio ($[\text{Na}/\text{Fe}] = +0.88$), and E3 stars present Na abundances similar to the remaining stars.

The stars we analyzed thus belong to the FG, and we found no evidence of stars belonging to the SG. E3 is therefore domi-

nated by FG stars. According to Fig. 22 of Milone et al. (2017), the fraction of FG stars in E3 is indeed expected to exceed 60% ($M_V = -4.12$, $1.4 \times 10^4 M_\odot$). With our limited statistics, which is based on only four stars, we cannot exclude the presence of SG stars. For example, Dalessandro et al. (2016) observed five RGB stars in NGC121, all of which belong to the FG, while from photometry they were able to detect the presence of the SG and concluded that FG stars account for more than 65% of the total cluster mass; however, in NGC121 SG stars are more centrally concentrated than FG stars. This, combined with the target selection from the outer cluster regions and the higher incidence of FG stars, favors the bias toward the observation of the latter. Our results are also consistent and support the results of SS15, who analyzed the CH-CN band in low-resolution spectra of 23 RGB stars and found no evidence of MPs in E3.

We measured Mg abundances in only two stars (#67 and #107) by spectroscopy of the strong, saturated line at 5711.083 \AA . The $[\text{Mg}/\text{Fe}]$ abundance ratios in the two stars differ by 0.3 dex, to be compared with estimated uncertainty of 0.11–0.14 dex. Dispersion in Mg abundances are observed in GCs, and participate in the observed anti-correlations (e.g., Pancino et al. 2017). Magnesium spreads are, however, usually less pronounced than Na spreads (Pancino et al. 2017), whereas we did not observe any spread in Na. We note that the difference in the EW of the two lines ($\sim 10 \text{ m\AA}$) is compatible with the expected errors of 3.6 and 6.2 m\AA for stars #107 and #67, respectively, and that part of the 0.3 dex difference in the $[\text{Mg}/\text{Fe}]$ abundance ratio originates from the difference in the measured iron content. Given the uncertainties involved in the present analysis, the observed variation in Mg abundance between stars #67 and #107 has to be considered as only tentative and wait for confirmations from additional analysis.

Figure 5 shows the E3 α -element abundance ratios ($[\text{Ti}/\text{Fe}]$, $[\text{Ca}/\text{Fe}]$, $[\text{Si}/\text{Fe}]$, and $[\text{Mg}/\text{Fe}]$ filled squares) versus $[\text{Fe}/\text{H}]$ in comparison with Galactic stars. In the figure, gray filled circles are halo stars from Gratton et al. (2003, their dissipative component) and Venn et al. (2004, halo probability greater than 0.8). Open magenta triangles are thick disk stars from Reddy et al.

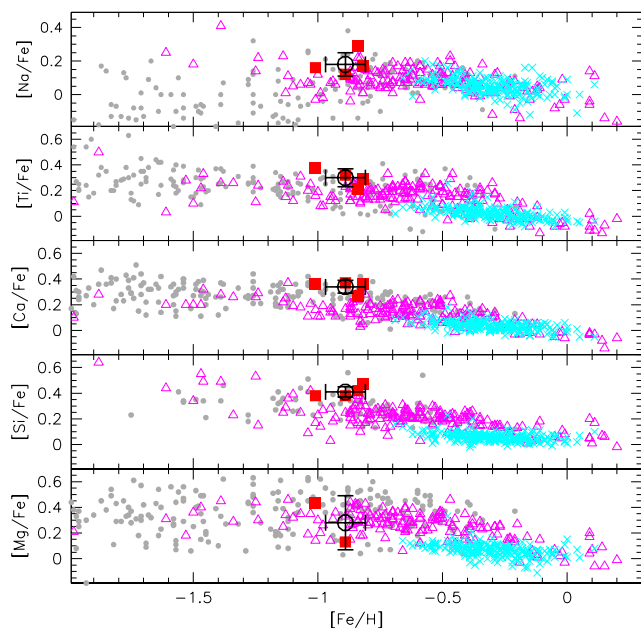


Fig. 5. Run of $[\text{Na}/\text{Fe}]$ and α -element abundance ratios ($[\text{Ti}/\text{Fe}]$, $[\text{Ca}/\text{Fe}]$, $[\text{Si}/\text{Fe}]$, $[\text{Mg}/\text{Fe}]$ from top to bottom) vs $[\text{Fe}/\text{H}]$ for E3 (filled red squares) and Galactic stars. The large black open circle with error bars indicates the mean cluster abundance and Gaussian dispersion. Gray filled circles are halo stars from Gratton et al. (2003, their dissipative component) and Venn et al. (2004, halo probability greater than 0.8). Open magenta triangles are thick disk stars from Reddy et al. (2006), while cyan crosses are thin disk stars from Reddy et al. (2003).

(2006), while cyan crosses are thin disk stars from Reddy et al. (2003). The $[\text{Mg}/\text{Fe}]$ abundance ratio of star #67 appears low, but it is within the observed trend. The mean cluster abundance ratios (large empty circles with error bars) are, in all cases, well within the observed Galactic trends, with enhancements consistently between ~ 0.3 and 0.4 dex. Agreement with the Galactic trends are also observed for the abundance ratios over Fe of Na (upper panel in Fig. 5), iron-peak elements (V, Cr, Mn, and Ni, Fig. 6) and neutron capture elements (Y, Ba, and Eu, Fig. 7).

We measured the yttrium abundance of star #107 only by spectroscopy of two lines. The abundances of the two lines differ by about 0.3 dex (-0.08 and 0.19 dex) and we provide the values for the individual lines in Table 2. The two values are compatible within the uncertainty estimated for each line (0.21 and 0.28 dex, see Table 3). The bottom panel of Fig. 7 shows that both values are compatible with the Galactic trend, with the lower value given by the YII line at 509 nm giving a better match.

The upper panel in Fig. 7 presents the $[\text{Ba}/\text{Y}]$ versus $[\text{Fe}/\text{H}]$ abundance ratio of star #107 in comparison with the Galactic trend. We again plot the abundance ratio, considering separately the abundances obtained for the two Y lines. This ratio is commonly used to discriminate the trend observed in Galactic stars with respect to that observed in stars born in Milky Way satellite galaxies (Sbordone et al. 2015). E3 follows the trend observed in Galactic stars.

5. Summary and conclusions

Based on high-resolution spectra obtained with FLAMES-UVES/VLT, we presented a chemical abundance analysis of four stars that are likely members of the globular cluster E3.

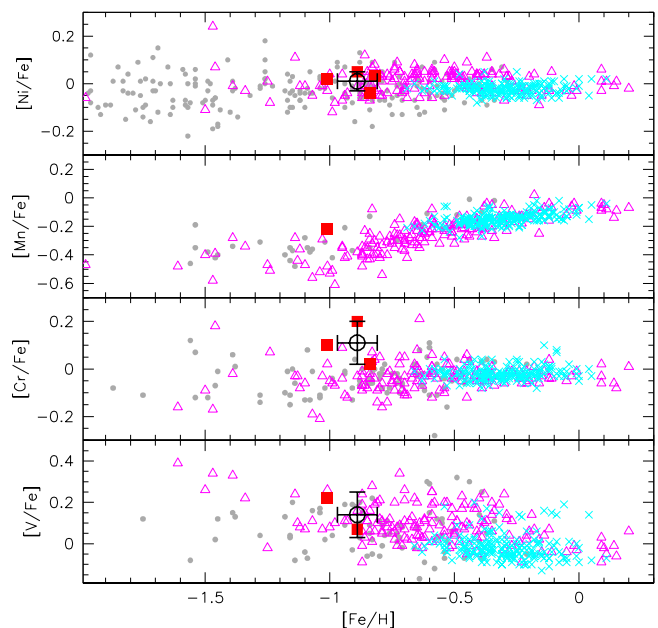


Fig. 6. Run of iron peak element abundance ratios ($[\text{Ni}/\text{Fe}]$, $[\text{Mn}/\text{Fe}]$, $[\text{Cr}/\text{Fe}]$, $[\text{V}/\text{Fe}]$ from top to bottom) vs $[\text{Fe}/\text{H}]$ for E3 and Galactic stars. Symbols are the same as in Fig. 5.

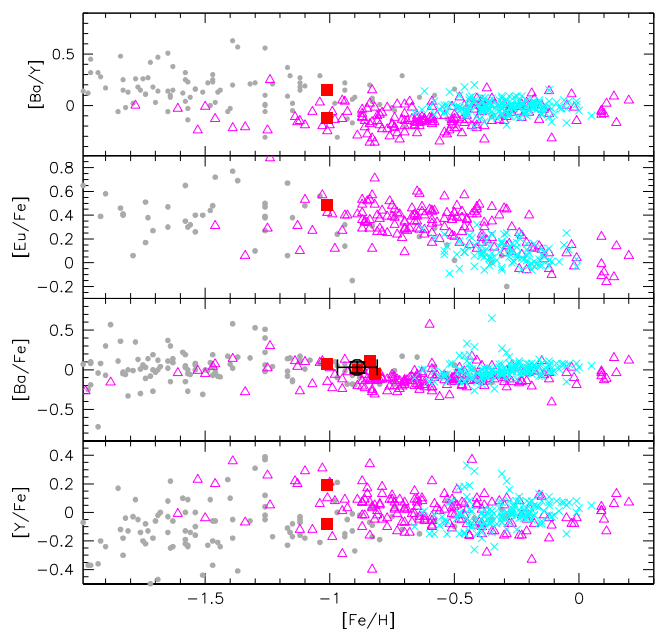


Fig. 7. Run of neutron capture element abundance ratios ($[\text{Ba}/\text{Y}]$, $[\text{Eu}/\text{Fe}]$, $[\text{Ba}/\text{Fe}]$, $[\text{Y}/\text{Fe}]$ from top to bottom) vs $[\text{Fe}/\text{H}]$ for E3 and Galactic stars. Symbols are the same as Fig. 5.

The mean heliocentric cluster radial velocity and metallicity are $v_{\text{helio}} = 12.6 \pm 0.4$ km ($\sigma = 0.6 \pm 0.2$ km s^{-1}) and $[\text{Fe}/\text{H}] = -0.89 \pm 0.08$ dex. This RV is consistent with the 8.9 ± 4 km s^{-1} reported by SS15 from low-resolution spectroscopy. The iron content is in good agreement with the FM15 value, which is however deduced from the spectroscopy of two stars whose RV is significantly different from our values, namely 45 ± 5 km s^{-1} .

We have presented abundances of the light element Na, iron-peak (Fe, V, Cr, Ni, Mn), α (Mg, Si, Ca, Ti), and neutron-capture (Y, Ba, Eu) elements. Mn, Y, and Eu abundances were only measured for star #107, having the highest S/N spectrum. E3 has abundance ratios of its α , iron-peak, and neutron-capture elements that are fully compatible with the trends observed in Galactic stars, and its α -enhancement is typical (0.3–0.4 dex) for a halo GC.

We did not detect any significant spread in Na abundance. The mean cluster Na abundance is $[\text{Na}/\text{Fe}]=0.18\pm 0.07$ dex, with a range between 0.12 and 0.29 dex, i.e., less than 0.2 dex. This mean value and observed spread place E3 in the portion of the Na-O diagram (Fig. 4) occupied mainly by FG stars and is close to the separation between FG and SG stars for the similar metallicity clusters M4 and 47 Tuc and the intermediate- and low-mass clusters NGC 288 and NGC 6535. The Na abundance of E3 stars is also similar to FG stars in the low-mass cluster Ter 8.

With a luminosity and mass slightly lower than E3 ($M_V=-4.12$, $M=1.4\times 10^4 M_\odot$, SS15, Harris 1996), Simpson et al. (2017) detected evidence of multiple populations in the GC ESO452-SC11 ($M_V=-4.02$, $M=6.8\times 10^3 M_\odot$). They suggest that most of the stars they observed in this cluster, appear to belong to the SG based on their high CN index strengths. Indeed, E3 stars appear to show low CN index strength compared with NGC1851 and ESO452-SC11 (see Fig.11 of Simpson et al. 2017).

We conclude that E3 is dominated by FG stars, consistently with what is expected on the basis of its low luminosity (Milone et al. 2017). Our results support the SS15 conclusion that E3 may be a single stellar population cluster. The easiest interpretation suggests that the low mass of the cluster did not allow the polluters from which SG stars would have formed to be retained. However, our limited statistics do not allow us to exclude the presence of a minor component of SG stars.

While mass is commonly considered an important factor for the development of MPs, others have been found to be relevant, such as age and metallicity and probably the environment (Carretta et al. 2010; Bastian & Lardo 2017). In addition to E3, a few more low-mass GCs are known that do not present evidence of MPs. Pal12 and Ter7 ($M_V=-4.47$, -5.01 , Cohen 2004; Sbordone et al. 2007) are known to belong to the Sagittarius dwarf spheroidal galaxy (Sgr dSph) or to have once been part of this galaxy. They are also known to be younger than the bulk of the Galactic GCs (Marín-Franch et al. 2009). The old, low-mass Sgr cluster Ter 8 ($M_V=-5.07$) also hosts a minority of SG stars and is dominated by FG stars (Carretta et al. 2014). Rup 106, similarly to E3 (FM15), has an age typical of the bulk of Galactic GCs, but it has also been suggested that it has abundance patterns pointing towards an extragalactic origin (Villanova et al. 2013). It is currently the most massive ($M_V=-6.35$) Galactic GC known not to host MPs. On the other hand, a number of relatively massive ($M\approx 10^5 M_\odot$) clusters younger than about 2 Gyr have been found that do not host MPs (Mucciarelli et al. 2008, 2014; Martocchia et al. 2017; Bastian & Lardo 2017; Martocchia et al. 2018).

The body of evidence accumulated so far supports E3 as a globular cluster dominated by first-generation stars, and having age and chemical composition similar to the bulk of the Galactic GC population.

Acknowledgements. We thank the anonymous referee and the editor Eline Tolstoy for a careful reading of the paper and constructive comments which improved the quality of the presentation. L.M. acknowledges support from “Proyecto Interno” of the Universidad Andres Bello. S.V. and C.M.B. gratefully acknowledge the support provided by FONDECYT N.1170518 and 1150060, respectively. This research has made use of the NASA As-

trophysics Data System and of the SIMBAD database, operated at CDS, Strasbourg, France. This work has made use of data from the European Space Agency (ESA) mission *Gaia* (<https://www.cosmos.esa.int/gaia>), processed by the *Gaia* Data Processing and Analysis Consortium (DPAC, <https://www.cosmos.esa.int/web/gaia/dpac/consortium>). Funding for the DPAC has been provided by national institutions, in particular the institutions participating in the *Gaia* Multilateral Agreement.

References

- Alonso, A., Arribas, S., & Martínez-Roger, C. 1999, *A&AS*, 140, 261
 Bastian, N., & Lardo, C. 2017, *arXiv:1712.01286*
 Bessell, M. S. 1983, *PASP*, 95, 480
 Bonifacio, P., Monai, S., & Beers, T. C. 2000, *AJ*, 120, 2065
 Bragaglia, A., Gratton, R. G., Carretta, E., et al. 2012, *A&A*, 548, A122
 Bragaglia, A., Carretta, E., D’Orazi, V., et al. 2017, *A&A*, 607, A44
 Bressan, A., Marigo, P., Girardi, L., et al. 2012, *MNRAS*, 427, 127
 Carretta, E., Bragaglia, A., Gratton, R. G., et al. 2009a, *A&A*, 505, 117
 Carretta, E., Bragaglia, A., Gratton, R., & Lucatello, S. 2009b, *A&A*, 505, 139
 Carretta, E., Bragaglia, A., Gratton, R. G., et al. 2010, *A&A*, 516, A55
 Carretta, E., Bragaglia, A., Gratton, R. G., et al. 2014, *A&A*, 561, A87
 Carretta, E., Bragaglia, A., Lucatello, S., et al. 2018, *arXiv:1801.09689*
 Cayrel, R. 1988, *The Impact of Very High S/N Spectroscopy on Stellar Physics*, 132, 345
 Coelho, P., Barbuy, B., Meléndez, J., Schiavon, R. P., & Castilho, B. V. 2005, *A&A*, 443, 735
 Cohen, J. G. 1978, *ApJ*, 223, 487
 Cohen, J. G. 2004, *AJ*, 127, 1545
 Dalessandro, E., Massari, D., Bellazzini, M., et al. 2014, *ApJ*, 791, L4
 Dalessandro, E., Lapenna, E., Mucciarelli, A., et al. 2016, *ApJ*, 829, 77
 Decressin, T., Meynet, G., Charbonnel, C., Prantzos, N., & Ekström, S. 2007, *A&A*, 464, 1029
 de la Fuente Marcos, R., de la Fuente Marcos, C., Moni Bidin, C., Ortolani, S., & Carraro, G. 2015, *A&A*, 581, A13 (FM15)
 D’Ercole, A., D’Antona, F., & Vesperini, E. (2016), *MNRAS*, 461, 4088
 Dekker, H., D’Odorico, S., Kaufer, A., Delabre, B., & Kotzłowski, H. 2000, *Proc. SPIE*, 4008, 534
 Gaia Collaboration, Prusti, T., de Bruijne, J. H. J., et al. 2016, *A&A*, 595, A1
 Gaia Collaboration, Brown, A. G. A., Vallenari, A., et al. 2018, Accepted for *A&A Special Issue on Gaia DR2* (*arXiv:1804.09365*)
 Gratton, R. G., Carretta, E., Eriksson, K., & Gustafsson, B. 1999, *A&A*, 350, 955
 Gratton, R. G., Bonifacio, P., Bragaglia, A., et al. 2001, *A&A*, 369, 87
 Gratton, R. G., Carretta, E., Claudi, R., Lucatello, S., & Barbieri, M. 2003, *A&A*, 404, 187
 Harris, W. E. 1996, *AJ*, 112, 1487 (2010 edition)
 Kurucz, R. L. 1993a, CD-ROM 13, 18 <http://kurucz.harvard.edu>
 Lupton, R., 1993. *Statistics in theory and Practice* (Princeton Un. Press)
 Marín-Franch, A., Aparicio, A., Piotto, G., et al. 2009, *ApJ*, 694, 1498
 Marino, A. F., Villanova, S., Piotto, G., et al. 2008, *A&A*, 490, 625
 Martocchia, S., Bastian, N., Usher, C., et al. 2017, *MNRAS*, 468, 3150
 Martocchia, S., Cabrera-Ziri, I., Lardo, C., et al. 2018, *MNRAS*, 473, 2688
 Milone, A. P., Piotto, G., Bedin, L. R., et al. 2012, *A&A*, 540, A16
 Milone, A. P., Piotto, G., Renzini, A., et al. 2017, *MNRAS*, 464, 3636
 Mucciarelli, A., Carretta, E., Origlia, L., & Ferraro, F. R. 2008, *AJ*, 136, 375
 Mucciarelli, A., Dalessandro, E., Ferraro, F. R., Origlia, L., & Lanzoni, B. 2014, *ApJ*, 793, L6
 Mucciarelli, A., Dalessandro, E., Massari, D., et al. 2016, *ApJ*, 824, 73
 Mucciarelli, A., Lapenna, E., Ferraro, F. R., & Lanzoni, B. 2018, accepted for publication in *ApJ* (*arXiv:1803.09759*)
 Pancino, E., Rejkuba, M., Zoccali, M., & Carrera, R. 2010, *A&A*, 524, A44
 Pancino, E., Romano, D., Tang, B., et al. 2017, *A&A*, 601, A112
 Pasquini, L., Avila, G., Blecha, A., et al. 2002, *The Messenger*, 110, 1
 Pasquini, L., Mauas, P., Käuff, H. U., & Cacciari, C. 2011, *A&A*, 531, A35
 Reddy, B. E., Tomkin, J., Lambert, D. L., & Allende Prieto, C. 2003, *MNRAS*, 340, 304
 Reddy, B. E., Lambert, D. L., & Allende Prieto, C. 2006, *MNRAS*, 367, 1329
 Renzini, A., & Fusi Pecci, F. 1988, *ARA&A*, 26, 199
 Renzini, A., D’Antona, F., Cassisi, S., et al. 2015, *MNRAS*, 454, 4197
 Salinas, R., & Strader, J. 2015, *ApJ*, 809, 169 (SS15)
 Sarajedini, A., Bedin, L. R., Chaboyer, B., et al. 2007, *AJ*, 133, 1658
 Sbordone, L., Bonifacio, P., Castelli, F., & Kurucz, R. L. 2004, *Memorie della Società Astronomica Italiana Supplement*, 5, 93
 Sbordone, L., Bonifacio, P., Buonanno, R., et al. 2007, *A&A*, 465, 815
 Sbordone, L., Monaco, L., Moni Bidin, C., et al. 2015, *A&A*, 579, A104
 Schlafly, E. F., & Finkbeiner, D. P. 2011, *ApJ*, 737, 103
 Schlegel, D. J., Finkbeiner, D. P., & Davis, M. 1998, *ApJ*, 500, 525

- Simpson, J. D., De Silva, G., Martell, S. L., Navin, C. A., & Zucker, D. B. 2017, MNRAS, 472, 2856
- Snedden, C. 1973, ApJ, 184, 839
- Taylor, M. B. 2005, Astronomical Data Analysis Software and Systems XIV, 347, 29
- Venn, K. A., Irwin, M., Shetrone, M. D., et al. 2004, AJ, 128, 1177
- Veronesi, C., Zaggia, S., Piotto, G., Ferraro, F. R., & Bellazzini, M. 1996, Formation of the Galactic Halo...Inside and Out, 92, 301 (V96)
- Villanova, S., & Geisler, D. 2011, A&A, 535, A31
- Villanova, S., Geisler, D., Carraro, G., Moni Bidin, C., & Muñoz, C. 2013, ApJ, 778, 186
- Villanova, S., Monaco, L., Moni Bidin, C., & Assmann, P. 2016, MNRAS, 460, 2351